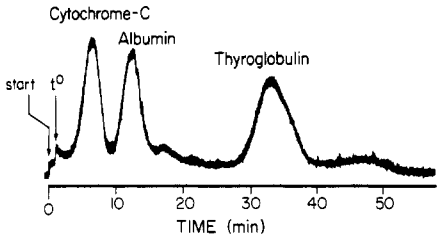

Figure 10. Separation of cytochrome *c*, albumin, and thyroglobulin in an asymmetrical system using opposing flow relaxation with $z' = 4.0$ cm, relaxation/focusing time (preceding "start") = 23 min ($\tau(95\%) = 10$ min), and cross flowrate = 3.1 mL/min. Flowrates during elution are $\dot{V}_{out} = 1.69$ mL/min and $\dot{V}_c = 3.24$ mL/min. Retention ratios were 0.20, 0.10, and 0.04, which gave diffusion coefficients of 1.2×10^{-6}, 6.0×10^{-7}, and 2.3×10^{-7} cm²/s, respectively.

ACKNOWLEDGMENT

We are grateful to P. Stephen Williams for assistance with computer calculations and some mathematical derivations.

LITERATURE CITED

(1) Giddings, J. C. *Anal. Chem.* **1981**, *53*, 1170A.
(2) Wahlund, K.-G.; Winegarner, H. S.; Caldwell, K. D.; Giddings, J. C. *Anal. Chem.* **1986**, *58*, 573.
(3) Giddings, J. C.; Myers, M. N.; Caldwell, K. D.; Fisher, S. R. In *Methods of Biochemical Analysis*; Glick, D., Ed.; Wiley: New York, 1980; Vol. 26, p 79.
(4) Giddings, J. C.; Yang, F. J.; Myers, M. N. *Anal. Chem.* **1976**, *48*, 1126.
(5) Lee, H.-L.; Reis, J. F. G.; Dohner, J.; Lightfoot, E. N. *AIChE J.* **1974**, *20*, 776.
(6) Giddings, J. C. *Sep. Sci. Technol.* **1986**, *21*, 831.
(7) Giddings, J. C. In Treatise *on Analytical Chemistry*; Kolthoff, I. M., Elving, P. J., Eds.; Wiley: New York, 1981; Part I, Vol. 5, Chapter 3.
(8) Giddings, J. C.; Yang, F. J.; Myers, M. N. *Science (Washington, D.C.)* **1976**, *193*, 1244.
(9) Yang, F. J.; Myers, M. N.; Giddings, J. C. *Anal. Chem.* **1977**, *49*, 659.
(10) Hovingh, M. E.; Thompson, G. H.; Giddings, J. C. *Anal. Chem.* **1970**, *42*, 195.
(11) Giddings, J. C. *Anal. Chem.* **1986**, *58*, 735.
(12) Giddings, J. C. *Anal. Chem.* **1985**, *57*, 945.
(13) Giddings, J. C.; Yang, F. J.; Myers, M. N. *Anal. Biochem.* **1977**, *81*, 395.

RECEIVED for review November 5, 1986. Accepted January 29, 1987. This work was supported by Grant No. GM10851-29 from the National Institutes of Health and was presented in part at the Tenth International Symposium on Column Liquid Chromatography, San Francisco, CA, May 18-23, 1986.

Retention by Electrical Field-Flow Fractionation of Anions in a New Apparatus with Annular Porous Glass Channels

Joe M. Davis, F.-R. F. Fan, and A. J. Bard*

Department of Chemistry, University of Texas at Austin, Austin, Texas 78712

A new apparatus for electrical field-flow fractionation (EFFF) studies utilizing annular porous Vycor glass (PVG) tubes to define a channel between external carbon and internal platinum electrodes is described. The anions poly(styrenesulfonate) and chromium phthalocyaninetetrasulfonate were retained by EFFF in four annular PVG channels having different channel widths with either high- or low-conductivity aqueous carrier. Experimental retention ratios depart considerably from predictions based on the theoretical EFFF parameter λ, and the departures cannot be explained by channel dead volume, solute relaxation, electroosmotic flow, or screening of the anionic charge by counterions. Results are partially explained by large solute transference numbers and polarization of carrier by the electric field. Experimental plate heights nevertheless agree well with theoretical expectation, when λ is estimated from experimental retention ratios and retention theory. The available PVG tubes are probably too rough to attain retention ratios much smaller than 0.35 and the PVG surface becomes pitted during column use, seriously limiting column lifetime and reproducibility.

Electrical field-flow fractionation (electropolarization chromatography) is a subtechnique of the chromatographic-like separation family, field-flow fractionation (FFF), in which charged species (e.g., ions, proteins, polyelectrolytes, or colloids) are concentrated near the wall of an open channel by an electric field and are differentially transported through the channel by laminar flow. Following sample injection, each species relaxes in the applied field toward one channel wall (the accumulation wall) and forms a quasi-equilibrium concentration distribution (zone) whose characteristic thickness depends (in the simplest case) on temperature and the electrical force on the constituent members of the species. Zones tightly localized near the wall are transported by flow less rapidly than the less localized zones, because the flow is less rapid near the channel walls than in the channel midsection. The fundamental principles of FFF have been detailed elsewhere (*1-4*).

In spite of numerous efforts (*5-12*), the three-component protein separation originally communicated by Caldwell et al. (*5*) and later refined by Kesner et al. (*7*) is the best multicomponent separation by electrical field-flow fractionation (EFFF) reported to date. Given the apparent difficulty in developing a useful EFFF system, further research seems justifiable only if such a system has desirable features lacking in other multicomponent separation methods based on free flow electrophoresis, such as flat fluid band (or fluid curtain or free flow) electrophoresis, continuous flow and density gradient isoelectric focusing, and capillary isotachophoresis and zone electrophoresis. Some minor shortcomings of these methods are noted here to highlight more fully several potential advantages of EFFF. Flat fluid band electrophoresis, although widely used for preparative biological separations, is largely limited by resolution (*13*). Separations based on continuous flow and gradient density isoelectric focusing are relatively slow and frequently require more than 1 day to complete (*14*); they are further complicated by the need to separate the resolved species from the ampholytes that form the pH gradients characteristic of the methods. The small column volumes encountered in capillary isotachophoresis and (especially) zone electrophoresis necessitate the use of so-

0003-2700/87/0359-1339$01.50/0

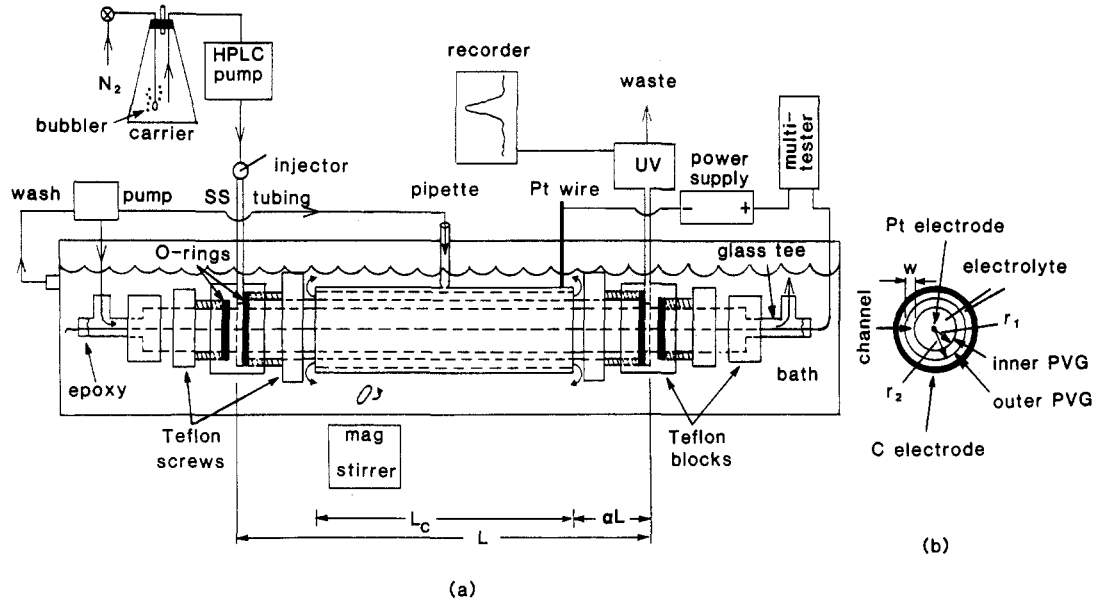

Figure 1. (a) Schematic of EFFF channel constructed from PVG and ancillary apparatus. (b) Cross-sectional side view of channel.

phisticated injection and detection devices (as in capillary LC) and preclude preparative-level separations. Capillary electrophoresis has deservedly attracted much attention because of its high efficiency (*15–18*), but the system's peak capacity is fundamentally limited by the electroosmotic (electroendosmotic) flow that sweeps out the capillary contents.

In contrast, a well-designed EFFF system constructed from inert materials, if one can generalize from more successful FFF methods, should be capable of the rapid high-resolution analytical- or preparative-scale fractionation of mixtures using conventional LC injectors and detectors. High-resolution separations should be attainable in short times by tightly focusing zones at the accumulation wall and rapidly pumping carrier through the channel. Preparative-scale fractionations should be possible with little loss in resolution by increasing the channel cross section while keeping the channel gap small. Furthermore, the peak capacity of EFFF is fundamentally unlimited by the elutive nature of the separation process. In addition, either a steady-state or variable electric field could be used (*19*); the latter would permit separations based on transport parameters as well as charge. These combined features are sufficiently attractive to warrant continued effort to develop a near-ideal system or, failing that, to discover and characterize the fundamental limitations prohibiting its development.

A number of inherent problems must be solved in designing a useful EFFF apparatus. The electrodes that are used to impose the field are in contact with the electrolyte solution and will, of necessity, have faradaic reactions occurring at their surfaces. If the channel walls are defined by these electrode surfaces, gas production at them will disrupt the formation of zones. Moreover corrosion of the electrodes can occur, causing roughening of the surfaces. While it might be possible to minimize such effects by judicious choice of solution–electrode reactions or by forming a suitable layer on the electrode surface (e.g., a conductive polymer with a high electrical capacity), initial experiments in our laboratory with polypyrrole-coated stainless steel electrodes were unsuccessful (*20*). A truly versatile apparatus will probably require that the electrodes be separated from a flow channel defined by a porous separator or an ionically conducting membrane. In previous EFFF apparatus, the channels were defined by dialysis membranes or ultrafiltration fibers (*5–12*). However, for good performance, the channel walls must be very smooth and the separators must be rigid enough to maintain a uniform channel over the full channel length, while permitting sufficient ion flow to yield a significant potential drop across the flowing electrolyte. The separator material should also be chemically inert and not adsorb solution components; the latter would lead to chromatographic effects superimposed on the EFFF process.

We report here the retention by EFFF of the anions poly(styrenesulfonate) (PSS) and chromium phthalocyaninetetrasulfonate (CrPcTS) in annular channels formed from concentric tubes of porous Vycor glass 7930 (PVG), a highly porous glass network of 40-Å-diameter pores (*21*) that permit the transport of small ions. A schematic representation of this EFFF configuration is shown in Figure 1. The study was restricted to anionic species because PVG, a strong cation exchanger (*22*, *23*), strongly adsorbed cationic species (e.g., $Ru(bpy)_3^{2+}$, methyl viologen, and Cr^{3+}). The anions were retained in four PVG channels having different gap widths using both buffered and unbuffered aqueous carrier. The results for CrPcTS are the first reported for the retention by EFFF of a species that is not a polyelectrolyte. Overall the results unfortunately fall well short of realizing the potential of EFFF noted above.

THEORY

The simplicity of the mathematical functions for the perpendicular electric field and the velocity profile in EFFF columns has facilitated the derivation of fairly rigorous equations governing zone migration and dispersion. The average velocity v of a species in any form of FFF is usually measured relative to the average linear velocity $\langle v \rangle$ of the carrier by retention ratio R (*24*)

$$R = \frac{v}{\langle v \rangle} = \frac{\langle c^* v \rangle}{\langle c^* \rangle \langle v \rangle} = \frac{V^\circ}{V_R} = \frac{t^\circ}{t_R} \qquad (1)$$

where c^* is the quasi-equilibrium concentration distribution, v is the velocity profile of the carrier, V° is the column void volume, t° is the time required to pump one void volume through the channel, V_R is the retention volume, or volume of eluant corresponding to the first moment of the peak generated by the species, and t_R is the time required to elute volume V_R. The broken brackets indicate that c^* and v are averaged over the channel cross section.

The exact form of R depends on the channel type and electrode configuration, which determine c^* and v. Equations for R have been derived for an open parallel-plate channel

Table I. Characterization of EFFF Channels

channel	V°(geometric),[a] cm^3	w,[a,b] μm	L_c, cm	L, cm	ρ_1	α	preparation of PVG
A	2.22 ± 0.06	610 ± 20	9.52	15.62	0.85	0.19	acid activated
B	2.33 ± 0.07	610 ± 20	9.52	16.36	0.85	0.21	virgin
C	7.79 ± 0.24	1020 ± 30	13.97	21.59	0.84	0.18	virgin
D	8.05 ± 0.25	1020 ± 30	13.97	22.86	0.84	0.19	virgin

[a] V° and w were calculated from 43 measurements made with dial calipers (±10 μm error) of the outer and inner diameters of the inner and outer tubes. Standard deviations were calculated by propagation of errors. [b] The small-gap (large-gap) channel was constructed from 7 and 10 (10 and 15) mm o.d. PVG.

(OPPC) (*24*) and a cylindrical ultrafiltration fiber (*6*) immersed in a uniform electric field E and for an annular channel immersed in a radial field (*25*). The OPPC R is the simplest and is

$$R = 6\lambda(\coth(2\lambda)^{-1} - 2\lambda) \tag{2}$$

where

$$\lambda = \frac{D_1}{|U|w} = \frac{D_1}{|\mu E|w} = \frac{l}{w} \tag{3}$$

In eq 3, D_1, U, and μ are the lateral diffusion coefficient, field-induced velocity, and electrophoretic mobility of a species and are assumed to be constant. Quantity l is the characteristic zone thickness and w is the distance between the two channel walls.

The Nernst–Einstein equation for mobility μ is (*26*)

$$\mu = zeD_1/kT \tag{4}$$

where e is the electronic charge and z is the signed number of such charges. Thus eq 3 can be also written as

$$\lambda = \frac{kT}{e|zE|w} = \frac{kT}{e|z\Delta V|} \tag{5}$$

where $\Delta V = Ew$ is the potential difference across gap w. Thus λ can be expressed as the ratio of the thermal energy kT that opposes zone formation to the magnitude of the electrical work $ze\Delta V$ that favors zone formation. Note that, as opposed to electrophoresis, where both molecular parameters z and D_1 affect the transport of an ionic species, in EFFF the effect of D_1 is absent. (D_1 would influence zone transport if the electric field were varied with time (*19*).)

Although the channels used here are annular, the more complicated R derived for them differs by only 6.2% or less from eq 2 (*25*), which is consequently used for simplicity. Gap w for these channels equals $r_2 - r_1 = r_2(1 - \rho_1)$, where r_2 and r_1 are the radii of the larger and smaller tubes and $\rho_1 = r_1/r_2$.

When extracolumn effects (e.g., injector and detector dead volume) are negligible, peak (zone) dispersion in FFF is principally dictated by the differential transport by flow of a zone's constituent members. The dispersion expected in a cylindrical fiber (*27*) and an OPPC (*28*) has been evaluated and can be expressed for the latter geometry as the nonequilibrium contribution H_n to plate height

$$H_n = \frac{\psi(\lambda)l^2v}{D_z} = \frac{\psi(\lambda)l^2R\langle v\rangle}{D_z} \tag{6}$$

where ψ is a mathematically complicated coefficient defined elsewhere (*28*) that approaches the value 4 as λ approaches zero and D_z is the (constant) axial diffusion coefficient. (Equation 6 is strictly the long-time limit for H_n, which must otherwise be evaluated numerically for "short" times (*29*).) H_n is clearly reduced by reducing zone thickness l, i.e., by decreasing R.

Equations 2 and 6 were derived by assuming that distribution c^* describes the zone's lateral concentration along the full channel length. A characteristic time $\tau = w/U = \lambda w^2/D_1$ is required for the zone constituents to relax into the steady-state distribution (*30*). When a zone is transported by flow prior to this relaxation process, the R and H_n expected are greater than the above predictions, because zone species are transported by widely differing velocities during relaxation (*24*, *31*). Analytical corrections to R and H_n exist only for the $\lambda \to 0$ limit (*24*); general corrections must be obtained approximately (*24*) or numerically (*32*).

Relaxation effects can frequently be eliminated by applying the field for a time $>\tau$ after introduction of sample into the channel but prior to the commencement of flow (*30*). For our apparatus shown in Figure 1, however, the channel fraction inside the carrier entrance and exit blocks is virtually insulated from the field, and departure from the above equations is inevitable. An approximate correction to R that is analogous to the R correction for solute relaxation proposed by Hovingh et al. (*24*) is presented here to account for this "dead volume".

If relaxation effects are negligible (and data presented later suggest that they are), to a first approximation a solute will migrate at carrier velocity $\langle v\rangle$ through the entrance block, quickly relax to the velocity v characteristic of its quasi-equilibrium distribution, and then migrate through the exit block with some characteristic velocity $\bar{v} = v + n(\langle v\rangle - v)$ between v and $\langle v\rangle$, where $0 \le n \le 1$. If α equals the fractional channel length inside either insulating block, the times, t_1 and t_2, the solute spends inside the entrance and exit blocks are $t_1 = \alpha L/\langle v\rangle$ and $t_2 = \alpha L/\bar{v}$, where L equals the channel length. Similarly, the time t_3 for which solute experiences the field is $(1 - 2\alpha)L/v$. The total time t_R that solute is retained is $t_R = t_1 + t_2 + t_3$. Since the time t° corresponding to a void peak is $L/\langle v\rangle$, the experimentally observed retention ratio R^* is related to $R = v/\langle v\rangle$ by

$$R^* = \frac{t^\circ}{t_R} = \frac{V^\circ}{V_R} = \frac{R}{1 - \alpha(2 - R - (1 + n(R^{-1} - 1))^{-1})} \tag{7}$$

An analogous general correction to nonequilibrium plate height H_n is considerably more complicated, even for the $\lambda \to 0$ limit. Equation 6 necessarily underestimates H_n for this channel because zones are also considerably broadened by flow in the carrier entrance and exit blocks, in which zone thickness l approaches infinity. As is shown below, however, reasonable agreement is nevertheless found between experimental plate heights and eq 6, which is consequently used here as a conservative estimate for H_n.

EXPERIMENTAL SECTION

PVG tubes (7, 10, and 15 mm nominal outside diameters) were obtained from Corning Glass Works (Corning, NY) and were used as received or following surface modification (see below). The characterizing features of the four EFFF channels constructed from these tubes are reported in Table I.

The PVG tubes were held rigidly in an annular configuration by two Teflon blocks, tapped and drilled as shown in Figure 1. The smaller tube passed through both blocks, whereas the ends of the larger tube terminated inside the blocks, adjacent to the $^1/_{16}$-in stainless steel tubing (0.020 in. i.d.) through which carrier entered and exited the channel. Leakage of the channel contents was prevented by rubber O-rings.

The radially symmetric electrodes were isolated from gap w to prevent bubbles formed during electrolysis from disrupting zone formation. The inner electrode (anode) was formed by centering and stretching tautly inside the inner tube a 0.127–0.5 mm Pt wire, which was epoxied to two borosilicate glass tees connected to the inner tube by Teflon blocks (see Figure 1). The outer electrode (cathode) was formed by clamping together around the larger PVG tube two half-cylindrical pieces of graphite, which were made by first drilling out a graphite rod (Ultra Carbon Corp., Sherman, TX) and then halving it. Electrical contact to the graphite was made with a Pt wire. These electrodes form essentially equipotential surfaces; it was estimated that only 1.25 V or so would be dropped over the full Pt wire length under the worst of possible conditions (current, 525 mA; Pt wire diameter, 0.127 mm).

The channel and electrodes were submerged in a stirred bath containing electrolyte (initially) identical in composition with the carrier fluid. The bath was continuously circulated over the electrodes to reduce polarization from gas bubbles.

The conductivities of the column influent and effluent and of the bath were measured with a RC-16B-1 conductivity bridge (Industrial Instruments, Cedar Grove, NJ) operating at 1 kHz. The bath conductivity was found to increase with time (especially for low-conductivity baths), most probably because of slow decomposition of the graphite electrode. (An IR spectrum of a methylene chloride extract of one bath contained sharp bands in the carbon fingerprint region.) A fresh bath was consequently prepared after one to five experiments, depending upon the bath composition. The decomposition of the carbon electrode was greatly accelerated by reversing the electrode polarity (i.e., Pt, –; C, +), which precluded outer-wall retention studies.

Unbuffered solutions of the sodium salts of PSS (ICN Pharmaceuticals, Inc., Plainview, NY; Polysciences, Inc., Washington, PA) and the potassium salts of CrPcTS were prepared from deionized water (MQ) generated by a Milli-Q reagent water system. Solutions buffered at pH 8.0 were prepared from reagent grade KH_2PO_4 and KOH and deionized water. Solute concentrations ranged from 0.8 to 2.5 mg/mL. No more than 25 μL of sample solution was injected at one time.

The carrier was introduced to the column by a Perkin-Elmer LC-65T liquid chromatography pump. Solutes were injected, using a 25-μL Hamilton syringe, onto the column via a 7125 Rheodyne sample injector and were detected by a Perkin-Elmer LC-65T UV–vis detector operating at 240 nm. A constant dc voltage was impressed across the electrodes by a Harrison 6205B dual power supply (Hewlett-Packard, Palo Alto, CA) or a variable power supply (General Radio Co., Cambridge, MA). Currents were measured with a range doubler multitester (Radio Shack, Fort Worth, TX). Fractograms were recorded by an Omnigraphic 3000 recorder (Houston Instruments, Austin, TX) and digitized manually with a Hipad digitizer (Houston Instruments). Peak areas and first and second moments were estimated from these digitized fractograms.

The surface of the PVG was chemically modified to compare the performance characteristics of modified and virgin PVG. First the siloxanes formed during the glass manufacture were hydrolyzed in 1 M HNO_3 (90 °C for 1 h). After being washed repeatedly with deionized water, the PVG was either used directly or further modified by reaction with halosilanes or poly(ethylene glycol) (PEG). The former procedure was carried out by bubbling dry N_2 through liquid triethylbromosilane (Aldrich Chemical Co., Milwaukee, WI) or *n*-octyldimethylchlorosilane (Petrarch Systems, Bristol, PA) and passing the diluted vapors for 48–120 h through a 160 °C silanized glass tube containing acid-treated PVG previously dried under vacuum ($<10^{-4}$ torr at 160 °C). The latter modification was carried out by bonding a 4000-molecular-weight PEG (Anspec Co., Ann Arbor, MI) to acid-treated PVG via γ-glycidoxypropyltrimethoxysilane (Aldrich), using the procedure reported by Chang et al. (*33*).

The macroscopic surface roughness of PVG was characterized with a JEOL JSM 35C scanning electron microscope and a Sloan Dektak profilometer having a 25-μm-diameter stylus.

PROCEDURES

The ranges of the observable retention ratios R^* of PSS and CrPcTS are reported in Table II as eight data sets. The R^* values were calculated from the first moments V_R of the solutes' elution profiles and eq 7; the appropriate geometrical void volumes V° are reported in Table I. The corrected ratios R were then calculated from these R^* values and eq 7, using the α values reported in Table I. The quantity n in eq 7 was set to zero, so that the resultant R's slightly overestimate the true ones.

To access the agreement between experimental and theoretical R's, the former were plotted against $(\Delta V)^{-1}$, the reciprocal of the estimated potential difference across gap w. This potential difference was not measured (e.g., by inserting electrical probes in the channel) because the voltage so measured would equal ΔV plus two potential drops of unknown magnitude across the double layers at the probe-solution interfaces; ΔV alone cannot be measured. The field (and potential) distribution in the gap is theoretically governed by the current density, carrier conductivity, and geometrical properties of the annulus (exclusive of the few angstroms over which the potential also drops across PVG–solution interfaces), which are known or presumably measurable. Assuming the field distribution was uniform (this assumption will be examined later), ΔV was estimated as

$$\Delta V = IR_a = \frac{I}{\sigma}\frac{\ln (1/\rho_1)}{2\pi L_c} \tag{8}$$

where R_a, σ, and L_c are the resistance of a uniform annulus, the average conductivity of the column effluent and the bath, and the carbon electrode length, respectively. (The ranges of I, σ, and ΔV are reported in Table II; L_c values are reported in Table I.) The data set $((\Delta V)^{-1}, R)$ was then fit using nonlinear least squares to the following modified form of eq 2

$$R = \frac{6A}{\Delta V}\left(\coth\left(\frac{2A}{\Delta V}\right)^{-1} - \frac{2A}{\Delta V}\right) \tag{9}$$

Examination of eq 2, 3, 5, and 9 shows that A should equal $kT/|z|e = D_l/|\mu|$. The expected and least-squares A values are reported in Table II as the ratio $Y = |z|eA/kT = |\mu|A/D_l$. Y is less than, equal to, or greater than unity when R is less than, equal to, or greater than the prediction of eq 2.

Plate heights H were calculated from the second moment σ_V^2 of the profile about mean V_R as (*35*)

$$H = L(\sigma_V^2/V_R^2) \tag{10}$$

(Column lengths L are reported in Table I.) Henceforth H is identified with the nonequilibrium plate height H_n. It is also assumed that $D = D_l = D_z$.

Peak area was found to decrease with increasing field strength. To characterize this decrease, the area of each retained peak was divided by the average area of several peaks generated under zero-field conditions (i.e., void peaks) to obtain a relative peak area, RPA. The data set (ΔV,RPA) was then fit to a straight line using least squares. The slopes (s), intercepts (i), and correlation coefficients (r) of these fits are reported in Table II.

RESULTS AND DISCUSSION

Figure 2 is a plot of the R's of sets A–H vs. –log (ΔV). The curves are the least-squares fits of sets A, C, D, and F–H to eq 9. (For reasons discussed below, the five largest ΔV data were excluded from the least-squares fits.) The following was deduced from this figure and Table II. (a) All R's are larger than those predicted by theory ($Y > 1$), even after first-order corrections for "dead volume". (b) As ΔV is increased, R decreases, levels out at $R \approx 0.35$ over a small ΔV range, and then increases (sets A and F). Peak area nonetheless decreases linearly with increasing ΔV even after R has leveled out. (c) PSS70K (the "70K" designates a number-average molecular

Table II. Experimental Conditions for Data Sets A–H

data set	sample	symbol[a]	column	electrolyte	V° (moments analysis), cm^3	I, mA	σ, Ω^{-1}·m^{-1}	ΔV, V	R^*	Y	RPA study
A	PSS70K	●	B	MQ	2.69 ± 0.18 (6)[b]	0.085–14.7	(0.95–2.2) × 10^{-4}	0.023–22.6	0.34–0.80	358[c]	i = 0.99; s = −0.046; r = −0.96
B	PSS70K	△	A	phosphate		185–525	0.42–0.51	0.056–0.17	0.41–0.48		i = 1.05; s = −1.63; r = −1.00[d]
C	PSS16K	◔	C	MQ		6.4–10.8	(3.0–6.9) × 10^{-4}	2.9–4.3	0.42–0.61	215[c]	
D	PSS70K	○	C	MQ	8.54 ± 0.00 (2)	2.9–12.3	(3.2–4.4) × 10^{-4}	1.7–6.0	0.31–0.57	147[c]	
E	PSS200K	◪	C	MQ		4.4	4.2 × 10^{-4}	2.0	0.41		
F	CrPcTS	▶	D	MQ	7.81 ± 0.10 (3)	0.64–26.9	(1.6–7.9) × 10^{-4}	0.67–15.0	0.39–0.85	51.4	i = 0.99; s = −0.064; r = −0.92
G	CrPcTS	□	D	phosphate	8.04 ± 0.68 (4)	30–150	0.12–0.13	0.046–0.23	0.86–0.91	10.1	i = 1.13; s = −2.26; r = −0.99
H	CrPcTS	■	A	phosphate	2.11 ± 0.08 (7)	185–525	0.44–0.55	0.11–0.30	0.76–0.93	9.8	i = 0.95; s = −0.42; r = −0.95

[a] Symbols represent the indicated data sets in Figure 2. [b] Number of replicates. [c] Based on $D/\mu \approx 1.4 \times 10^{-3}$ V. [d] Based on two data.

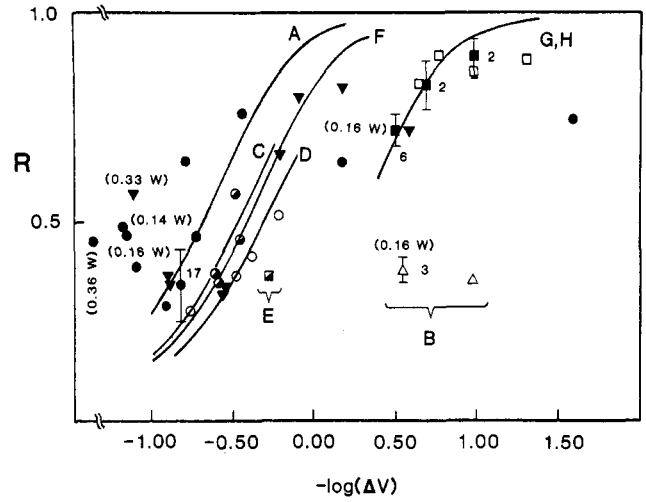

Figure 2. Plot of R vs. −log (ΔV) generated from retention of PSS and CrPcTS. The curves are the least-squares fits of eq 9 to data sets detailed in Table II; a single curve depicts the fits to sets G and H. Numbers adjacent to points with error bars and in parentheses indicate the numbers of times experiments were repeated and the estimated powers dissipated within the channel as heat, respectively.

weight equal to 70 000) in MQ (set D) is only retained slightly more than PSS16K in MQ (set C) and is retained more in a large-gap (set D) than in a small-gap (set A) channel. PSS200K in MQ (set E) is retained somewhat more than the other PSSs in MQ (sets A, C, and D). (d) The R's of CrPcTS in MQ (set F) are comparable to those of PSSs in MQ. (e) The R's of PSS70K in MQ (set A) and CrPcTS in MQ (set F) are roughly independent of small ΔV values over the examined ΔV range. (f) The R's of buffered CrPcTS are approximately equal in small-gap (set H) and large-gap (set G) channels and most closely agree with theory.

As is shown further below, theoretical H_n values calculated from eq 6 using λ's estimated from experimental R's and eq 2, and l's from these λ's and eq 3, agree fairly well with experimental H values, even though $Y > 1$. Since H_n depends on λ and l (see eq 6), both parameters must be estimated fairly well to give agreement with experiment. The l's so estimated from the minimum retention ratio in Figure 2, $R \approx 0.35$ ($\lambda \approx 0.067$), are 40 and 68 μm in the small- and large-gap channels, respectively. Evidence nonetheless exists that l values smaller than these were experimentally realized. Assuming that the adsorption sites of PVG were never saturated during an experiment, the finding that peak area decreases with increasing ΔV, even after R has plateaued, indicates that solute is increasingly concentrated at the inner-tube wall. The concentration increases because the zone is more tightly focused at the accumulation wall, i.e., because l decreases. In the plateau region, however, R does not decrease with decreasing l, in contrast to the predictions of eq 2 and 3. An explanation consistent with both observations is that the minimum R value is dictated not by the magnitude of l but by the number of multiple relaxations zone species must undergo near a rough PVG surface (*24*). To support this assertion, it is noted that the l's calculated above are roughly twice the standard deviations of the gap widths reported in Table I and are consequently on the order of the standard deviations of the inner-tube radii. In general, a zone will be repeatedly distorted from its quasi-equilibrium distribution if it is carried by flow over a "roller coaster" of elevations and dips comparable in size to itself. Each distortion results in solute relaxation, which increases R; here, such relaxations are so numerous that they govern the minimum R value.

An alternative explanation for the plateau of R values is the polarization by the field of electrolyte ions, which can cause R to plateau in weakly conducting electrolytes, such as these

(*9, 11*). This is unlikely because the R's of highly buffered PSS70K (set B) are comparable to the R's in the plateau region.

R eventually increases as ΔV is further increased most probably because of ohmic heating and free convection. The electrical power $(\Delta V)^2/R_a$ dissipated within the channel as heat was calculated for each datum in Figure 2 and is largest for the largest ΔV values. (Some large powers are reported in the figure; such data were excluded from least-squares fits to eq 9.) Judging from the data, convection cannot be excessive, since zone formation is only disturbed slightly. A feeling for the amount of convection expected is gained by calculating an upper limit to the free-convective Nusselt number Nu for the experiment corresponding to the largest ΔV datum of set F, following the procedure of Pohl (*34*). From the upper limit ΔT to the temperature change over gap w

$$\Delta T = \sigma(\Delta V)^2/2\kappa \tag{11}$$

the Prandtl number $\mathrm{Pr} = C_p\mu^*/\kappa$ of water, and the Grashof number Gr of the annular system

$$\mathrm{Gr} = g\beta\Delta T w^3/(\mu^*/\rho)^2 \tag{12}$$

the Nu = Nu(Pr,Gr) number of the annular system could in principle be determined experimentally. (Symbols are defined in the Glossary.) Rather than do this, the Pr and annular Gr values calculated from the equations above were used to evaluate the Nusselt numbers corresponding to cylinders (Nu = 1.1), plates (Nu = 1.6), and spheres (Nu = 3.3) immersed in a uniform fluid (*36*). The annular Nu is probably comparable. These Nu's, on the order of unity, indicate that convection is minor, in agreement with experimental observation.

The departure of sets G and H from theory is surprising, since these R's are relatively large and should be more free of perturbations from wall effects than other data. This departure cannot solely be attributed to "dead volume" effects because setting parameter n in eq 7 to one (i.e., recalculating R from R^* assuming solute moves through the exit block with velocity $\langle v \rangle$) changes the reported R values by only −18% or less. Nor can the relaxation of solute to the accumulation wall explain the large but almost equal Y values, because relaxation time τ depends on w^2 for fixed λ (or ΔV) and the w's of channels A and D differ by the factor 1.7.

One possible origin of departure is the electroosmotic flow (EOF) that moves through the PVG capillary pores from anode to cathode (at pH 8), a direction opposite to field-induced velocity U. The volumetric flow rate $\dot{V}$ of carrier through the pores is proportional to current I (*37*) and consequently is largest in high-current experiments (such as these). This explanation is unrealistic because, as observed above, the Y values of sets G and H are similar, but the current ranges differ by roughly a factor of 3. In other words, the 3-fold change in $\dot{V}$ does not affect solute migration rate.

Additional evidence that EOF does not disturb zone formation was found experimentally by disconnecting column C from the carrier pump and measuring the rates at which a 0.001 M phosphate buffer (pH 6.05, $\sigma = 0.11\ \Omega^{-1}\cdot m^{-1}$) flowed out of the column at different currents. (The bath is the origin of the flowing liquid, since the column does not empty.) A linear relationship between $\dot{V}$ and I was found ($r = 0.95$), with slope $\dot{V}/I = 2.2 \times 10^{-9}\ m^3/(A\cdot s)$. This ratio is an underestimation of the potentially zone-disrupting EOF through the inner-tube pores since a fraction of this flow must also exit as EOF through the outer-tube pores. Assuming that this underestimation was minimal (see below), a series of EOF velocities was calculated as $\dot{V}/A'$, where $A' = 2\pi r_1 L_c$ is the inner-tube surface area exposed to field E. These velocities are 13% or less of the U's calculated from the experimental R's of sets G and H, eq 2 and 3, and the estimated D of CrPcTS, $5 \times 10^{-6}\ cm^2/s$, which was calculated from the Reddy and Doraiswamy equation (*40*). (The above assumption was justified by calculating the ζ potential at the pore/solution interface expected to produce the experimental V/I ratio, using the theories of Rice and Whitehead (*38*) and Morrison and Osterle (*39*). The calculated $\zeta = -89$ mV closely agrees with the ζ potential of vitreous silica in a pH 6, 0.001 M KNO_3 solution, −94 mV (*37*). Thus it appears that most EOF comes from the inner tube and flows out of the channel, which is consistent with the observation of Kesner et al. that flexible OPPCs are expanded by EOF accumulating in the channel (*7*).)

Table III. Data for Sample Calculations of Transference Number t_i

species	μ_j, $cm^2/(V\cdot s)$	z_j	c_j, M	pH
$H_2PO_4^-$	-3.73×10^{-4} (*55*)	−1	3.45×10^{-3} [a]	8.0
			0.0248	4.5
HPO_4^{2-}	-5.91×10^{-4} (*55*)	−2	0.0215[a]	8.0
			4.87×10^{-5}	4.5
K^+	7.62×10^{-4} (*26*)	1	0.0503	8.0
			0.025	4.5
CrPcTS	-7.7×10^{-4}	−4	9.65×10^{-4} [b]	8.0
albumin	1.3×10^{-5} (*8*)	0.57[c]	1.5×10^{-5} [d]	4.5

[a] Total phosphate concentration (i.e., $[H_3PO_4] + [H_2PO_4^-] + [HPO_4^{2-}] + [PO_4^{3-}]$) was 0.025 M. $[PO_4^{3-}]$ is negligible at these pHs. [b] c_s = 1.0 mg/mL; molecular weight = 1036 g/mol. [c] Calculated from eq 4 and $D = 5.9 \times 10^{-7}\ cm^2/s$ (*8*). [d] c_s = 1.0 mg/mL; molecular weight = 65 000 g/mol.

Sets G and H may furthermore depart from theory because no reduction in the effective CrPcTS charge due to screening of the anion by its counterion atmosphere was considered. The atmosphere thickness is relatively small in these concentrated electrolytes (12.7 Å in a pH 8.0, $\sigma \approx 0.45\ \Omega^{-1}\cdot m^{-1}$ phosphate buffer), and thus a substantial fraction of the counterion atmosphere will migrate with CrPcTS during its electrophoresis, reducing its charge. This fraction lies principally between the radius of the anion (estimated from its geometrical structure as 9.5 Å) and the radius of hydrodynamic shear (estimated as 5 Å larger than the sphere radius (*26*)). This fraction was evaluated from data comprising set H as 0.17, using a theory describing the spatial distribution of counterions (assumed to be point charges) in the diffuse double layer surrounding a charged sphere (*37*). This approximation suggests that the effective charge on CrPcTS may be only 80% or so of its formal charge ($z = -4$). Furthermore, there is the possibility that CrPcTS forms an ion pair with one of its counterions, which would reduce the formal charge of the anion by one unit. Both these changes in charge are relatively small, however, and can at best only account partially for the departures reported in Table II.

One reason that the R's of sets G and H differ from theory is the surprising nonuniformity of field E that exists because CrPcTS carries a nonnegligible fraction of current I, even in these highly conductive electrolytes. The fractional current carried in solution by CrPcTS, or generally by the ith species, equals its transference number t_i (*36*)

$$t_i = z_i\mu_i c_i / \sum_j z_j\mu_j c_j \tag{13}$$

where z_j, μ_j, and c_j are the charge, mobility, and concentration of the jth species in solution.

Simple calculations of t_i are given to illustrate this point. The required z_j, μ_j, and c_j values (the latter from set H) are reported in Table III. The concentrations of the various phosphate species and of potassium in the $\sigma \approx 0.45\ \Omega^{-1}\cdot m^{-1}$ buffer were estimated from multiple equilibria and charge balance equations. The CrPcTS concentration corresponds to that injected, equivalent to 1 mg/mL. The CrPcTS mo-

bility was estimated from $z = -4$, eq 4, and the diffusion coefficient of CrPcTS given earlier.

Based on these data, $t_i = 0.044$ for CrPcTS. In other words, over 4% of current I would be carried by CrPcTS, if the anion were distributed uniformly in solution. The fractional current attributable to CrPcTS migration in the zone vicinity is actually greater, because localization of CrPcTS at the inner-tube wall increases its concentration. A simple mass balance on a solute plug that neglects convective transport relates the inner-wall concentration c_i^* to the concentration c_s injected (25)

$$c_i^* = \frac{c_s}{2} \frac{(1 - \rho_1^2)(a + 2)\rho_1^a}{(1 - \rho_1^{a+2})} \qquad (14)$$

$$a = (\lambda \ln \rho_1)^{-1}$$

and predicts that $c_i^* = 5.9c_s$ for the smallest R of set H, $R = 0.72$ ($\lambda = 0.19$). Other quantities remaining equal, $t_i = 0.21$ for CrPcTS at the inner wall. A similar calculation shows that the uniformly distributed CrPcTS t_i for set G is 0.052, which roughly differs from the set H value by only 10%.

This phenomenon has not been reported previously, most probably because virtually all solutes used in earlier EFFF studies were proteins, for which μ_j and c_j are both relatively small due to the protein's high molecular weight. To justify this assertion, the inner-wall t_i of the protein albumin (c_s = 1 mg/mL) in a pH 4.5, $\sigma \approx 0.45\ \Omega^{-1}\cdot m^{-1}$ phosphate buffer calculated as above using additional data reported in Table III was only 1.4×10^{-4} (or 1500 times smaller than the inner-wall t_i for CrPcTS) for a well-retained albumin zone corresponding to $R = 0.20$.

The principal consequence of a large solute t_i is that the field E is reduced in the zone vicinity, because the current-carrying solute does not migrate through the glass. (No CrPcTS was ever found in the bath, whose UV–vis spectrum was periodically examined.) This phenomenon should be distinguished from the somewhat related field-reducing polarization of electrolyte ions discussed in detail by Lightfoot et al. (11), in which E is reduced by the buildup of electrolyte ions at the accumulation walls.

Curves A, C, D, and F in Figure 2 are the least-squares fits to eq 9 of R's generated from PSS and CrPcTS in MQ. It is clear from comparison of these fits and set E to curves G and H and set B that at fixed ΔV R increases as the carrier conductivity decreases, in agreement with earlier studies (9), probably because of large solute t_i's (for reasons detailed above) and the polarization of electrolyte at the accumulation wall (11). It is difficult to rationalize the apparently similar charges of the PSS and CrPcTS, even though polyelectrolytes immobilize counterions in their strong electrostatic fields (41), thus reducing their formal charges.

The PSS R's may in part be similar because the D/μ ratios of the polymers are similar. Although PSS of different molecular weight have been separated by polyacrylamide gel electrophoresis (42) (possibly because of sieving effects), their free-solution mobilities, equaling $\sim(2\text{–}4) \times 10^{-4}$ cm^2/(V·s), are largely independent of molecular weight, polymer concentration, and, to a first approximation, an added salt (41, 43–45). Even the PSS mobility at infinite dilution is not much larger, because the equivalent conductivity, Λ, of PSS solutions is almost concentration independent (46), in contrast to the sharp increase in Λ that is commonly observed as polyelectrolytes are diluted (which promotes increased dissociation of counterions) (41). The diffusion coefficients of PSS also differ by only a factor of 2–3 (assuming equal polymer concentrations) over the molecular-weight-range $(1\text{–}12) \times 10^5$ g/mol (41, 44, 49) but, unlike the mobilities, depend strongly on polymer concentration (47–49) and added salt (48). Even though the equations for R and H_n given earlier assume the lateral diffusion coefficient is constant, Hovingh et al. obtained good agreement between these equations and thermal FFF experiments (in which the lateral diffusion coefficient varies with temperature) by assigning to D_l the diffusion coefficient corresponding to the temperature of the zone's center of gravity (24). Here, in a similar manner, the value assigned to D_l was the diffusion coefficient corresponding to the concentration c_l of the zone's center of gravity, which is approximately $1/e$ times the inner-wall concentration c_i^* (24). The R's considered here are mostly less than 0.6 ($\lambda < 0.14$), and eq 14 predicts for these R's that $c_i^* > 8.2c_s$ or $c_l > 3.0$ mg/mL ($c_s > 1.0$ mg/mL). For polymer concentrations greater than 3–4 mg/mL, the diffusion coefficients of these PSSs in salt-free solutions are fairly independent of polymer concentration, approximately equaling 4.2×10^{-7} cm^2/s (47, 49). Consequently, the ratio $D/\mu \approx 1.4 \times 10^{-3}$ V does not vary much with molecular weight, which is consistent with the observation that the PSS R's are largely independent of molecular weight. (Clearly this does not fully explain the data because the CrPcTS D/μ ratio, 6.5×10^{-3} V, is 4.6 times larger than those for the PSSs but the R's of the two solutes are comparable.)

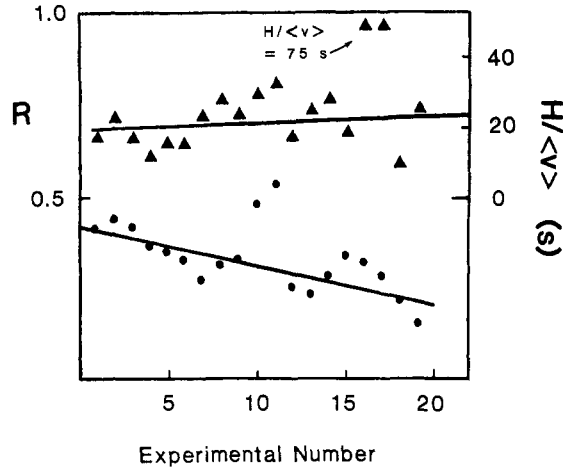

Figure 3. Plots of R and $H/\langle v \rangle$ vs. the experimental number, as generated from PSS70K in MQ. Solid lines are least-squares fits to these data, exclusive of the two largest R's and $H/\langle v \rangle$'s.

Although the expression $\lambda = D/|\mu \Delta V|$ is somewhat consistent with the experimental data, the λ expression derived from the Nernst–Einstein equation (eq 4), $\lambda = kT/e|z\Delta V|$, is clearly inconsistent, since the formal charge z of the PSS increases with molecular weight. (If this latter equation were valid, the PSS could be separated on the basis of molecular weight.) Manning has questioned the significance of calculating the charge of a high-molecular-weight polyelectrolyte from eq 4 because the electrophoretic and diffusive friction coefficients of the polyelectrolyte are not equal, as is assumed in eq 4 (50); the former corresponds to a freely draining polymer and the latter to a nondraining one.

The experimental reproducibility of R and H in PVG channels was investigated by retaining PSS70K in MQ (a subset of set A) 19 times over a 2-week period. By and large, the first nine experiments were not contiguous and were staggered among others comprising set A, whereas the latter ten were staggered among void-peak runs only. Figure 3 is the resultant plot of R and $H/\langle v \rangle$ vs. the experimental number (e.g., the abscissa, 12, represents data from the 12th experiment), which is proportional to time or column use. (Quantity $\langle v \rangle$, which spanned a 3.3-fold range, was calculated by dividing the carrier flow rate by the channel cross-section.) R clearly decreases with increasing experimental number but in an apparently cyclical manner, for reasons that are not presently understood. The line of negative slope is a least-squares fit to these data ($r = -0.79$). Furthermore, the R's generated by

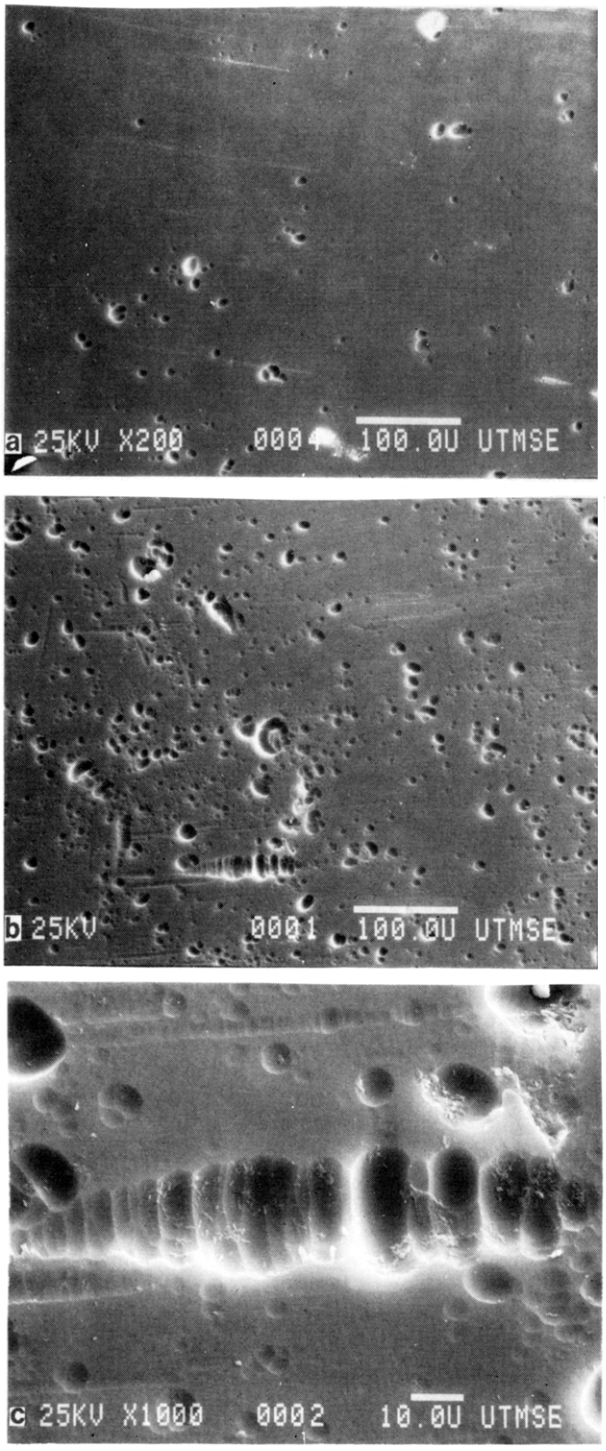

Figure 4. SEM photomicrographs of (a) virgin PVG (140×), (b) the inner tube of column B after 2 weeks of use (140×), and (c) the wormlike pit in the bottom center of Figure 4b, which contains particulate-like deposits (700×).

the final experiments are smaller than the minimum R value (0.35) reported earlier. The ratio $H/\langle v \rangle$ slightly increases uniformly with increasing experimental number.

These systematic changes in R and $H/\langle v \rangle$ can be explained in part by the SEM photomicrographs of the exterior surfaces of a 7-mm-o.d. virgin PVG tube (Figure 4a) and the inner tube from column B (Figure 4b), which was sacrificed after the reproducibility study. The latter surface is much more pitted than the former. A higher magnification of the pitted surface discloses small particulate-like deposits in the pits (Figure 4c), which also were found on the unpitted internal surface of the outer tube from column B but not on virgin PVG. The PVG that was insulated inside the carrier entrance and exit blocks was not as pitted as that exposed to the field, which suggests that pitting was accelerated by the field. Profilometry of the inner-tube surface revealed no extensive structure, indicating that the pit depth was considerably less than 25 μm (the stylus diameter).

All four PVG columns were transparent when assembled but slowly became translucent with increased use, probably due to the refraction and scatter of light from the pitted PVG surface. Since the decrease in transparency was gradual, one can infer that the extent of surface pitting increased with use, which qualitatively explains Figure 3. The R's and H's (or $H/\langle v \rangle$'s) of solutes retained in FFF channels modified by cutting grooves in the accumulation wall are known to be smaller and larger, respectively, than those obtained from unmodified channels (*51*). These R's and H's principally change because quiescent liquid in the grooves acts like a chromatographic stationary phase: solute molecules diffuse into the grooves and remain there until they diffuse out (to a first approximation). Increasing the groove density is analogous to increasing a column's stationary phase loading, which further decreases R and increases H. Here, the "grooving" (pitting) of PVG is not controlled or systematic but the system qualitatively behaves in an analogous way, i.e., R decreases and $H/\langle v \rangle$ increases as the surface becomes more pitted.

Since flat plates (rather than the cylindrical tubes used here) of PVG are commercially available, it should be possible to construct an OPPC channel from such plates, which could be polished with an abrasive grit (the glass is very soft) prior to assembly to reduce the R-limiting roughness of the tubes detailed above. The performance characteristics of such a channel were not explored because, as the study above shows, unmodified PVG does not exhibit the necessary long-term stability and reproducibility required of an ideal column material.

The acid activation of PVG had no apparent effect on R (refer to channels A and D in Table I and sets G and H in Table II), but the chemical derivatization of PVG by halosilane or PEG produced columns inferior in performance to unmodified ones. Both halosilane columns adsorbed much more solute than did virgin PVG, even under zero-field conditions. Even after several days of use, the effluent from the PEG-derivatized column was roughly 100 times more conductive than the MQ influent to the column, and well controlled low-conductivity studies were not possible. The adsorptivity of this column increased with use, and further characterization was stopped when solutes began to adsorb irreversibly.

The magnitudes of the slopes s reported in the final column of Table II indicate that the amount of solute adsorbed on PVG depends on (among other things) the solute type (cf. sets B and H) and the ionic strength (or conductivity) of the carrier (cf. sets F, G, and H; sets A and B). The extent of adsorption increases with ionic strength in part because the double layers around the solute and at the PVG/solution interface are compressed as the salt concentration increases, which reduces the electrostatic repulsion between the solute molecules and PVG (the glass is negatively charged at pH >3.5 (*52*)) and enables the two to approach closely, where short-range attractive forces (e.g., van der Waals) are important (*53*).

The area losses reported here should not be confused with similar ones reported previously (*9–11*) and attributed to electroretention (ER), the apparently "infinite" retention (i.e., $R \rightarrow 0$) of a solute fraction that is observed in an EFFF experiment until the electric field is turned off. Some ER was observed in roughly half of the experiments summarized in Table II, but only rarely did the recovered electroretained fraction exceed 10% of the corresponding void-peak area,

whereas the adsorption losses reported in Table II are much greater (as much as 90% of the void-peak area). Because comparable solute masses (e.g., ≈50 μg) were injected onto the PVG columns in this study and the ultrafiltration fibers used to study extensively ER, one wonders if ER depends more on solute concentration than mass, as previously suggested (*11*), since the fraction of material electroretained in the fibers was much greater than that in the PVG channels and the cross-sectional area of even the smaller PVG channel was 29 times greater than that of the fiber (*9*).

Even though experimental R's depart considerably from theoretical expectation, experimental H's agree fairly well with theoretical H_n's (or $H_n/\langle v \rangle$'s) computed from eq 6, λ's estimated from experimental R's and eq 2, and l's estimated from these λ's and eq 3. One particularly close agreement is found between the R's and $H/\langle v \rangle$'s depicted in Figure 3. The average R in the figure (R = 0.34) corresponds to λ = 0.056 and l = 34 μm (w = 610 μm), as calculated from eq 2 and 3. For this λ, the nonequilibrium coefficient $\psi = \psi(0.056) = 2.67$ (*28*). To calculate the expected ratio $H_n/\langle v \rangle = \psi l^2 R/D$, one further needs the diffusion coefficient of PSS70K in low-conductivity water (e.g., MQ). As stated earlier, the diffusion coefficient of salt-free PSS70K is roughly 4.2×10^{-7} cm^2/s when $R < 0.6$. From this value of D and the above data, the ratio $H_n/\langle v \rangle$ = 26 s was calculated from eq 6. This estimate agrees very well with the experimental $H/\langle v \rangle$ values (21 ± 6 s) depicted in Figure 3.

Fair agreement between experimental and theoretical H_n's was also found for the anion CrPcTS in MQ (set F). A series of constant ΔV experiments spanning a 2.6-fold range in $\langle v \rangle$ was carried out, from which a plot of H vs. $\langle v \rangle$ was generated. From the average retention ratio of these data, R = 0.66, the parameters λ = 0.16, l = 163 μm (w = 1020 μm), and $\psi(0.16)$ = 1.10 were estimated as above, and the theoretically expected slope $\psi l^2 R/D$ of the H vs. $\langle v \rangle$ plot was calculated to equal 35 s, using the CrPcTS diffusion coefficient $D = 5 \times 10^{-6}$ cm^2/s given earlier. The slope of the least-squares line fit to the experimental data (r = 0.78) was 58 s, or 64% larger than expected. While this error is considerably larger than for the PSS70K case above, it is not atypical of the errors encountered in previous plate-height studies in FFF (*54*).

Thus it appears that experimental results and the predictions of theory are internally consistent provided that the fundamental parameter λ is estimated from experiment and eq 2 instead of eq 2 and 5. The consistency suggests that zone formation, migration, and dispersion are occurring more or less normally but that field-induced velocity U is much smaller than that theoretically expected.

As stated earlier, the relaxation of solute to the accumulation wall had little effect on R in this study. When zone velocity is affected by relaxation, R increases with velocity $\langle v \rangle$. An approximate theory predicts that a plot of $1/R$ vs. $\langle v \rangle$ should be a straight line with a negative slope proportional in magnitude to relaxation time τ (*24*). Such a plot was generated from the CrPcTS data collected for the plate-height study reported above, but the slope of the least-squares line that was fit to these data was positive (i.e., R was actually somewhat larger at slower flow rates). A similar plot was made for the anion PSS70K in MQ, using a subset of set A; the experimental slope was almost zero. Thus relaxation is probably unimportant in these studies.

CONCLUSIONS

The discrepancies between experimental and theoretical R's cannot be explained by relaxation effects, electroosmosis, an electrostatic screening of the anions by their counterion atmospheres, or an incompleteness in addressing channel "dead volume" but are qualitatively explained by a reduction in field strength E due to polarization of electrolyte ions and large solute transference numbers. The semiquantitative treatment given here is inadequate to eliminate the possibility that other effects are also operative. It appears from these data to be primarily the description of E, and thus the theoretical λ, that is erroneous because internal consistency exists between plate-height and retention theories and experimental λ's.

Virgin and chemically modified PVG do not exhibit the inertness, reproducibility, and longevity that are prerequisite to the ideal EFFF column material. It is unlikely that this glass can be readily modified to eliminate these serious shortcomings.

ACKNOWLEDGMENT

The IMSL routine ZXMWD was used for least-squares minimization. The authors thank Michael Schmerling (of the University of Texas at Austin) for the profilometry and SEM studies, Wayne Riley (of Exxon) for the initial EFFF experiments, and Jack Kirkland (of Du Pont) for numerous helpful suggestions.

GLOSSARY

A	coefficient in eq 9
A'	inner-tube surface area exposed to field E
a	$(\lambda \ln \rho_1)^{-1}$
C_p	constant-pressure heat capacity of water
c^*	quasi-equilibrium concentration
c_i^*	inner-wall concentration
c_j	concentration of jth species in solution
c_l	center-of-gravity concentration
c_s	concentration of solute injected onto column
D	general diffusion coefficient
D_l	lateral diffusion coefficient
D_z	axial diffusion coefficient
E	constant field strength
e	elementary charge
Gr	Grashof number
g	acceleration due to gravity
H	experimental plate height
H_n	nonequilibrium plate height
I	current
i	intercept
k	Boltzmann's constant
L	channel length
L_c	carbon electrode length
l	characteristic zone thickness
Nu	Nusselt number
Pr	Prandtl number
R	retention ratio
R^*	experimentally observed retention ratio
R_a	macroscopic resistance of uniform annulus
r_1	inner-PVG-tube radius
r_2	outer-PVG-tube radius
r	correlation coefficient
s	slope
T	temperature
ΔT	maximum temperature drop across annulus
t°	void time
t_i	transference number
t_R	retention time
U	field-induced velocity
V°	void volume
V_R	retention volume
$\dot{V}$	volumetric flow rate due to EOF
v	velocity profile of carrier
$\langle v \rangle$	average linear velocity of carrier
$\bar{v}$	characteristic velocity of solute in exit block
ΔV	potential difference across annulus
w	channel width or gap
Y	$\lvert\mu\rvert A/D$
z	signed number of fundamental charges
α	fractional channel length inside insulating block
β	coefficient of volume expansion of water
ζ	zeta potential
κ	thermal conductivity of water

Λ	equivalent conductivity
λ	$D/\lvert u\Delta V\rvert$
μ	electrophoretic mobility
μ^*	viscosity of water
ν	zone velocity
ρ	density of water
ρ_1	r_1/r_2
σ	average conductivity of column effluent and bath
σ_v^2	second moment of peak about mean V_R
τ	relaxation time
ψ	nonequilibrium coefficient

ACRONYMS

CrPcTS	chromium phthalocyaninetetrasulfonate
EFFF	electrical field-flow fractionation
EOF	electroosmotic flow
ER	electroretention
FFF	field-flow fractionation
MQ	low-conductivity water from Milli-Q system
OPPC	open parallel-plate column
PEG	poly(ethylene glycol)
PVG	porous Vycor glass
PSS	poly(styrenesulfonate)
RPA	relative peak area
SEM	scanning electron microscope

LITERATURE CITED

(1) Giddings, J. C. *Sep. Sci. Technol.* **1984**, *19*, 831.
(2) Giddings, J. C.; Myers, M. N.; Caldwell, K. D. *Sep. Sci. Technol.* **1981**, *16*, 549.
(3) Giddings, J. C. *Anal. Chem.* **1981**, *53*, 1170A.
(4) Lightfoot, E. N.; Chiang, A. S.; Noble, P. T. *Annu. Rev. Fluid Mech.* **1981**, *13*, 351.
(5) Caldwell, K. D.; Kesner, L. F.; Myers, M. N.; Giddings, J. C. *Science* **1972**, *176*, 296.
(6) Reis, J. F. G.; Lightfoot, E. N. *AIChE J.* **1976**, *22*, 779.
(7) Kesner, L. F.; Caldwell, K. D.; Myers, M. N.; Giddings, J. C. *Anal. Chem.* **1976**, *48*, 1834.
(8) Giddings, J. C.; Lin, G.-C.; Myers, M. N. *Sep. Sci.* **1976**, *11*, 553.
(9) Chiang, A. S.; Kmiotek, E. H.; Langan, S. M.; Noble, P. T.; Reis, J. F. G.; Lightfoot, E. N. *Sep. Sci. Technol.* **1979**, *14*, 453.
(10) Shah, A. B.; Reis, J. F. G.; Lightfoot, E. N.; Moore, R. E. *Sep. Sci. Technol.* **1979**, *14*, 475.
(11) Lightfoot, E. N.; Noble, P. T.; Chiang, A. S.; Ugulini, T. A. *Sep. Sci. Technol.* **1981**, *16*, 619.
(12) Alam, T. M.; Russell, D. 37th Pittsburgh Conference and Exposition on Analytical Chemistry and Applied Spectroscopy, Atlantic City, NJ, March 1986; No. 734.
(13) Andrews, A. T. *Electrophoresis: Theory, Techniques, and Biochemical and Clinical Applications*; Clarendon Press: Oxford, 1981.
(14) Bours, J. In *Isoelectric Focusing*; Catsimpoolas, N., Ed.; Academic: New York, 1976; Chapter 8.
(15) Jorgenson, J. W.; Lukacs, K. D. *Science* **1983**, *222*, 266.
(16) Gassman, E.; Kuo, J. E.; Zare, R. N. *Science* **1985**, *230*, 813.
(17) Lauer, H. H.; McManigill, D. *Anal. Chem.* **1986**, *58*, 166.
(18) Walbroehl, Y.; Jorgenson, J. W. *Anal. Chem.* **1986**, *58*, 479.
(19) Giddings, J. C.; Caldwell, K. D. *Anal. Chem.* **1984**, *56*, 2093.
(20) Fan, F.-R. F.; Riley, W.; Bard, A. J., unpublished experiments, The University of Texas at Austin, 1984.
(21) Corning Glass Works, brochure on Porous Vycor Glass 7930, 1985.
(22) Wolfgang, S.; Gafney, H. D. *J. Phys. Chem.* **1983**, *87*, 5395.
(23) Wei, S.; Gafney, H. D.; Clark, J. B.; Perettie, D. J. *Chem. Phys. Lett.* **1983**, *99*, 253.
(24) Hovingh, M. E.; Thompson, G. H.; Giddings, J. C. *Anal. Chem.* **1970**, *42*, 195.
(25) Davis, J. M.; Giddings, J. C. *J. Phys. Chem.* **1985**, *89*, 3398.
(26) Bard, A. J.; Faulkner, L. R. *Electrochemical Methods: Fundamentals and Applications*; Wiley: New York, 1980; pp 67, 135.
(27) Reis, J. F. G.; Ramkrishna, D.; Lightfoot, E. N. *AIChE J.* **1978**, *24*, 679.
(28) Giddings, J. C.; Yoon, Y. H.; Caldwell, K. D.; Myers, M. N.; Hovingh, M. E. *Sep. Sci.* **1975**, *10*, 447.
(29) Krishnamurthy, S.; Subramanian, R. S. *Sep. Sci.* **1977**, *12*, 347.
(30) Giddings, J. C. *Anal. Chem.* **1985**, *57*, 945.
(31) Yang, F. J.; Myers, M. N.; Giddings, J. C. *Anal. Chem.* **1977**, *49*, 659.
(32) Jayaraj, K.; Subramanian, R. S. *Sep. Sci. Technol.* **1978**, *13*, 791.
(33) Chang, S. H.; Gooding, K. M.; Regnier, F. E. *J. Chromatogr.* **1976**, *120*, 321.
(34) Pohl, H. A. *Dielectrophoresis*; Cambridge University Press: Cambridge, 1978.
(35) Giddings, J. C. In *Treatise of Analytical Chemistry: Part I*, 2nd ed.; Kolthoff, I. M., Elving, P. J., Eds.; Wiley: New York, 1982; Vol. 5.
(36) Bird, R. B.; Stewart, W. E.; Lightfoot, E. N. *Transport Phenomena*; Wiley: New York, 1960.
(37) Hunter, R. J. *Zeta Potential in Colloid Science: Principles and Applications*; Academic: London, 1981.
(38) Rice, C. L.; Whitehead, R. *J. Phys. Chem.* **1965**, *69*, 4017.
(39) Morrison, F. A., Jr.; Osterle, J. F. *J. Chem. Phys.* **1965**, *43*, 2111.
(40) Sherwood, T. K.; Pigford, R. L.; Wilke, C. R. *Mass Transfer*; McGraw-Hill: New York, 1975.
(41) Armstrong, R. W.; Strauss, U. P. *Encycl. Polym. Sci. Technol.* **1969**, *10*, 781.
(42) Chen, J.-L.; Morawetz, H. *Macromolecules* **1982**, *15*, 1185.
(43) Nagasawa, M.; Noda, I.; Takahashi, T.; Shimamoto, N. *J. Phys. Chem.* **1972**, *76*, 2286.
(44) Meullenet, J.; Schmitt, A.; Drifford, M. *J. Phys. Chem.* **1979**, *83*, 1924.
(45) Nagasawa, M.; Soda, A.; Kagawa, I. *J. Polym. Sci.* **1958**, *31*, 139.
(46) Vink, H. *Makromol. Chem.* **1982**, *183*, 2273.
(47) Gruner, F.; Lehmann, W. P.; Fahlbusch, H.; Weber, R. *J. Phys. A: Math. Gen.* **1981**, *14*, L307.
(48) Koene, R. S.; Mandel, M. *Macromolecules* **1983**, *16*, 220.
(49) Koene, R. S.; Mandel, M. *Macromolecules* **1983**, *16*, 973.
(50) Manning, G. S. *J. Phys. Chem.* **1980**, *84*, 1059.
(51) Giddings, J. C.; Smith, L. K.; Myers, M. N. *Sep. Sci. Technol.* **1978**, *13*, 367.
(52) Bolt, G. H. *J. Phys. Chem.* **1957**, *61*, 1166.
(53) Marra, J.; van der Schee, H. A.; Fleer, G. J.; Lyklema, J. In *Adsorption from Solution*; Ottewill, R. H., Rochester, C. H., Smith, A. L., Eds.; Academic: London, 1983.
(54) Davis, J. M.; Giddings, J. C. *Sep. Sci. Technol.* **1985**, *20*, 699.
(55) Mason, C. M.; Culvern, J. B. *J. Am. Chem. Soc.* **1949**, *71*, 2387.

RECEIVED for review November 6, 1986. Accepted January 27, 1987. This work was supported by the Separations Research Program of the University of Texas at Austin.